Preequilibrium neutron emission in the reactions ^{90}Zr, ^{208}Pb(p,xn) with 80 MeV projectiles

M. Trabandt and W. Scobel
Institut für Experimentalphysik, Universität Hamburg, Hamburg, Federal Republic of Germany

M. Blann and B. A. Pohl
Lawrence Livermore National Laboratory, Livermore, California 94550

R. C. Byrd* and C. C. Foster
Indiana University Cyclotron Facility, Indiana University, Bloomington, Indiana 47405

R. Bonetti
Istituto de Fisica Generale Applicata dell'Universita di Milano, Milano, Italy
(Received 17 October 1988)

The reactions ^{90}Zr, ^{208}Pb(p,xn) have been measured with 80.5 MeV protons in the neutron continuum $E_n > 20$ MeV and the angular range $0° \leq \theta \leq 145°$. Whereas the angle-integrated spectrum can be explained by semiclassical preequilibrium models, this nucleon-nucleon scattering approach fails at far backward angles. In contrast, the quantum statistical multistep calculations give good agreement. They are indicative of a decrease of the effective nucleon-nucleon interaction with increasing nucleon energy.

I. INTRODUCTION

Spectral and angular distributions of continuum neutrons from (p,n) reactions are particularly appropriate for the study of the preequilibrium (PE) reaction phase, because a competing breakup mechanism as in the case of complex projectiles or inelastic projectile scattering that would complicate the interpretation of the data are excluded. In the last ten years, the equilibration process has been studied quite frequently with this reaction type[1–4] with projectile energies up to 45 MeV.

Several nuclear reaction models consider the equilibration to proceed through increasingly complex configurations of single-particle excitations. On one hand, there is the class of *semiclassical* models that apply the quasifree intranuclear transition rates. Among the most frequently used are the exciton[5] and hybrid[6] models which, though conceptually different,[7] yield convincing results for angle-integrated nucleon energy spectra, but which mostly fail to reproduce angular distributions in the backward hemisphere.[8,9] Suggested reasons for the latter include finite-size effects, incorrect treatment of higher chance nucleon emission, and incorrect balance of single versus multiple-nucleon emission.[11,12]

Quantum statistical models have been presented[11,12] that succeeded in describing the angular distributions of (p,n) and (p,p') data. In particular, the statistical multistep model[12] provides excellent agreement not only in the energy regime of prevailing multistep compound (SMCE) (Ref. 13) or direct (SMDE) (Ref. 14) emission, but also in the transition region with comparable contributions from both reaction types.[15] The residual interaction strength V_0 in this model has been brought to consistency[16] with direct reaction results. The phenomenological model of Kalbach[17] finally may be considered as a derivative of the exciton and the statistical multistep model.

The contribution of preequilibrium emission to the nucleon yield increases with projectile energy. Therefore, accurate (p,n) data for $E_p > 50$ MeV that extend with good energy resolution and low background to very backward angles would provide a crucial test of semiclassical and quantal preequilibrium models. These data, however, are scarce. Sakai *et al.*[18] studied ^{93}Nb(p,xn) for $E_p = 65$ MeV with emphasis on the analyzing power. Kalend *et al.*[19] performed (p,n) measurements for $E_p = 90$ MeV and several targets, but with somewhat poor resolution and the angular range 20°–135°. The Los Alamos–Jülich group presented data for $E_p = 318$ and 800 MeV and two angles (7.5° and 30°); additional measurements to energies E_p between 256 and 800 MeV for an extended ($\theta \leq 150°$) angular range are in progress.[20] Cierjacks *et al.*[21] studied several targets at $E_p = 585$ MeV and angles 30°, 90°, and 150°, but with poor energy resolution.

We have started a program to study the (p,n) continuum for $E_p = 80$, 120, and 160 MeV in the angular range 0°–145° for the targets ^{7}Li, ^{13}C, ^{27}Al, ^{90}Zr, and ^{208}Pb in extension of previous[1,4,22] measurements at lower projectile energies. The experiment has been designed to provide data with low background and γ contamination and with good energy resolution. In this paper, we present the first data obtained for $E_p = 80.5$ MeV and compare them with model calculations in order to (i) test the predictive power of the MSDE and MSCE models for angular distributions and the energy scaling[23] of the residual interaction strength V_0; (ii) have a look at the results of the hybrid model as a typical semiclassical formulation; and (iii) check whether the phenomenological description of multistep angular distributions[17] can be confirmed.

These comparisons will be presented in Sec. III after a description of some experimental details in Sec. II.

II. EXPERIMENTAL METHODS AND RESULTS

A. Time-of-flight facility

The experiment was performed at Indiana University Cyclotron Facility (IUCF) with the cyclotron operating at a frequency of 30.2 MHz. A burst separation of 1.8 μs was achieved by use of the stripper loop, a small isochronous storage ring for the d.c. beam from the ion source.[24] The long beam-off time allowed neutron time-of-flight (tof) spectroscopy with high resolution over a broad dynamic range: The suppression was controlled continuously to stay beyond 1:1000.

The 80.5-MeV proton beam had an average intensity of 14 nA and a burst width of $\Delta t \leq 700$ ps at the magnetic beam swinger[25] which was operated with deflection angles of 0°, 11°, and 24°, respectively. This allowed us to measure the angular range from 0° to 144° with five fixed detectors; the tof path lengths varied from 11.1 m for the most backward to 46.5 m for the most forward detector (see Table I). The detector which was used to measure angles of 82°–106° (laboratory angle) required a 15-cm diameter collimator hole to be cut through 1.2 m of concrete shielding. This collimator appeared visually to be slightly off the axis of the detector and target and to reduce the effective solid angle; the geometry required near perfect axial alignment to realize the full solid angle subtended by this detector. The spectra observed with this detector seem to be approximately a factor of 2 below those of the detectors covering the higher or lower angles, and we believe that this is the result of inaccurate alignment.

The neutron detectors consisted of cylindrical cells (30.5 cm diam $\times$ 20.3 cm) filled with the liquid scintillator BI501 (density $\rho = 0.901$ g/cm^{-3}, H/C ratio 1.287), with photomultiplier tubes RCA 8854 and voltage dividers optimized for good time resolution and n-γ discrimination.[26] The cells were coupled to the phototubes via partially[27] coated conical Lucite light pipes in a geometry equivalent to that of Ref. 28. Veto paddles made of oversized sheets of plastic scintillator were placed in front of all detectors to discriminate against protons, and on top of the three more backward detectors to suppress cosmic radiation.

The efficiencies $\eta(E_n, E^s_{\rm th})$ for neutrons of energies E_n and software thresholds $E^s_{\rm th}$ were calculated with the code of Cecil *et al.*[29] Independently, the detector efficiencies were determined from the 0° neutron yields for the ^{7}Li$(p,n)^7$Be transition to the ground and first excited state, which are the only particle-stable ones in ^{7}Be. Their absolute differential cross sections are known from the normalization of the integrated angular distributions to the total activation cross section.[30,31] A comparison between the experimental efficiencies and the calculated ones (that are used throughout this work) will be discussed elsewhere.[32]

B. experimental setup

The beam was focused on self-supporting targets with thicknesses ranging from 23 to 175 mg/cm^2 (see Table II). Behind them, the beam was magnetically deflected and dumped into a heavily shielded Faraday cup. Elastically scattered protons were detected with a ΔE-E telescope consisting of plastic scintillators. They allowed selection of the correct, phase locked timing signal from the cyclotron rf, which was used as a stop signal for the neutron tof spectroscopy.

The electronics used were conventional in nature. The linear biases $E^n_{\rm th}$ given in Table I were set individually in hardware for each detector. The calibration of the pulse height in terms of electron energies was obtained with the Compton edges of several γ sources with the maximum energy being attributed to the 90% point.[33] The light response function of Ref. 34 was used for conversion into proton energies.

Pulse shape discrimination of neutrons against γ radiation has been performed by measuring the time of the zero crossover generated from the integrated[26] anode signal with a delay line amplifier against the direct fast anode signal. Figure 1 shows the excellent discrimination features of this large detector and demonstrates at the same time the necessity of a software discrimination with a two-dimensional data replay.

From each event, the neutron tof, pulse height, pulse shape, and identification signal were registered. Some typical tof spectra resulting from runs with ^{90}Zr are shown in Fig. 2.

C. Measurements and data reduction

Each run was accompanied by a background run of about half its length. Background was measured by placing tubes of appropriate diameter filled with water as shadow bars midway between target and detectors; they generated flux attenuations of at least 99% for all neutron energies under consideration. In addition, some runs

TABLE I. Neutron detector data; ΔE_n is given for a time resolution $\Delta t = 2.5$ ns and $E_n = 60$ MeV (and a target of thickness $\Delta E_p = 600$ keV).

Detector no.	$\theta_{\rm lab}$ (deg)	tof (m)	$E^n_{\rm th}$ (MeV)	$E^s_{\rm th}$ (MeV)	ΔE_n (MeV)
1	0°, 11°, 24°	46.55	12.8	15	0.69 (0.91)
2	24°, 35°, 48°	38.43	11.6	14	0.84 (1.03)
3	45°, 56°, 69°	26.14	11.3	14	1.23 (1.37)
4	106°, 95°, 82°	14.92	11.0	12	2.16 (2.24)
5	144°, 133°, 120°	11.14	9.8	12	2.90 (2.96)

TABLE II. Target and reaction data. Excitation energies E^*(IAS) of the isobaric analogs are from Ref. 36.

Target	Thickness (mg/cm^2)	ΔE_p (MeV)	$Q(p,n_0)$ MeV	$E^*_{\rm IAS}$ (MeV)
^{7}Li	23.1;98	0.17;0.70	−1.64	0
^{13}C	102	0.79	−3.00	0
^{90}Zr	77.5;112	0.40;0.57	−6.89	5.11
^{208}Pb	71.4;175	0.29;0.72	−3.66	15.18

were performed with blank target frames that reproduced the background only in the unphysical region (see Fig. 2).

After n-γ discrimination, the tof spectra were converted into energy spectra in the center-of-mass frame with the detector efficiencies $\eta(E_n,E^s_{\rm th})$. The absorbing materials along the tof paths including the absorption in the air were taken care of by applying corrections on the basis of the energy-dependent reaction cross sections $\sigma_R(E_n)$.[35] The energy spectra resulting after background subtraction are shown in Figs. 3 and 4 for a selection of 10 out of the 15 angles and with 0.5 MeV binning. Both targets show the isobaric analog ground-state transitions (IAS), whose positions and widths (without binning), as well as those of the resolved transitions for ^{7}Li, ^{13}C(p,n) confirm the energy resolution stated in Table II.

The relative uncertainties within angular distributions are mostly due to target inhomogeneities (5%), inconsistencies in the background treatment (10%), and incomplete beam-current integration (4%). The estimated error margin is 14%. Absolute uncertainties include those of the detector efficiencies[32] and are slightly higher.

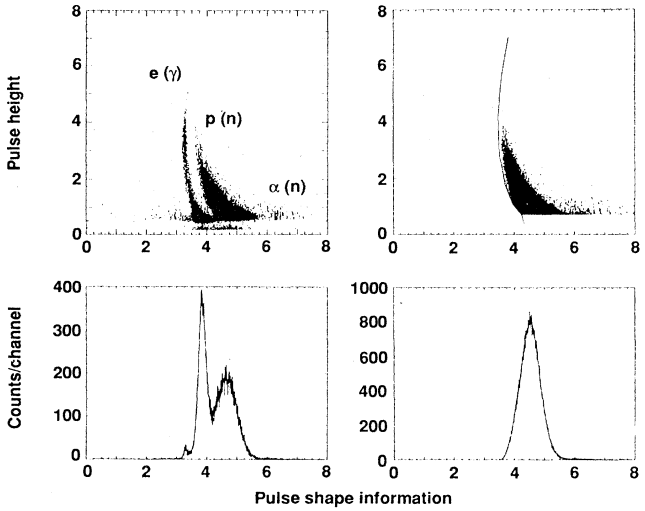

FIG. 1. *Top*: Scatter plots of pulse height (integrated anode signal) versus pulse shape signal and the software discrimination of neutrons. *Bottom:* Corresponding spectra of the pulse shape signal. Data are for 80.5-MeV protons on ^{208}Pb at $\theta_{\rm lab}=106°$.

III. RESULTS AND DISCUSSION

A. Statistical multistep model

We shall give here only an outline of the model[12] with emphasis on the parameters and assumptions entering into the numerical calculations to be presented. For details and explanation, the reader is referred to Refs. 13–15.

The double differential cross section of the SMCE contribution,

$$\frac{d^2\sigma}{dU\,d\Omega}=\sum\frac{(-1)^{s'-s}}{(2I+1)(2i+1)}\bar{Z}(lJlJ;sL)\bar{Z}(l'Jl'J;sL)P_l(\cos\theta)\frac{\pi}{k^2}\sum_{n=1}^{r}\sum_{\nu=n-1}^{n+1}\frac{\langle\rho_\nu(U)\Gamma_n^{\uparrow}(U)\rangle}{\Gamma_n}\left[\prod_{k=1}^{n-1}\right]\frac{\Gamma_k^{\downarrow}}{\Gamma_k}\frac{2\pi\Gamma_1}{D_1}\ , \quad (1)$$

increases with the residual excitation energy U and is symmetrically distributed around $\theta=90°$. The leading sum represents the correct angular momentum coupling (see Ref. 13). Figures 3 and 4, however, show that even for the lowest neutron energy, $E_n=20$ MeV, there is a pronounced asymmetry. Therefore, the SMCE contribution is expected to be rather small.

The continuum wave functions used to calculate the incident and escape widths Γ_1 and $\Gamma_n^{\uparrow}$ were generated using the proton optical-model potential of Ref. 37. The neutron optical-model potential was obtained from the previous one, by changing the sign of the asymmetry term. The bound-state shell-model wave functions were harmonic oscillator ones with holes h down to $1s_{1/2}$ and particles p up to $2f_{5/2}$.

As only particle bound states are involved in the SMCE process, the level density ρ_ν of the p-h configurations in the various steps calculated with the equidistant-spacing Fermi-gas model was cut whenever an excited particle exceeded the binding energy value. The validity of this approximation has been discussed in Ref. 15. All level densities were calculated with the single-particle level-density parameter $a=A/8.5$ MeV^{-1}, because shell closure effects are washed out[22] for all but the lowest excitation energies U.

The SMDE contribution was calculated using the expression

$$\frac{d^2\sigma}{dU\,d\Omega}=\sum_n\sum_{m=n-1}^{n+1}\int\frac{d\mathbf{k}_1}{(2\pi)^3}\cdots\int\frac{d\mathbf{k}_n}{(2\pi)^3}\left[\frac{dW_{m,n}(\mathbf{k}_f,\mathbf{k}_n)}{dU_f d\Omega_f}\right]\left[\frac{dW_{n,n-1}(\mathbf{k}_n,\mathbf{k}_{n-1})}{dU_n d\Omega_n}\right]$$
$$\times\cdots\left[\frac{dW_{2,1}(\mathbf{k}_2,\mathbf{k}_1)}{dU_2 d\Omega_2}\right]\frac{d^2\sigma_{1i}(\mathbf{k}_1,\mathbf{k}_i)}{dU_1 d\Omega_1}\ , \quad (2)$$

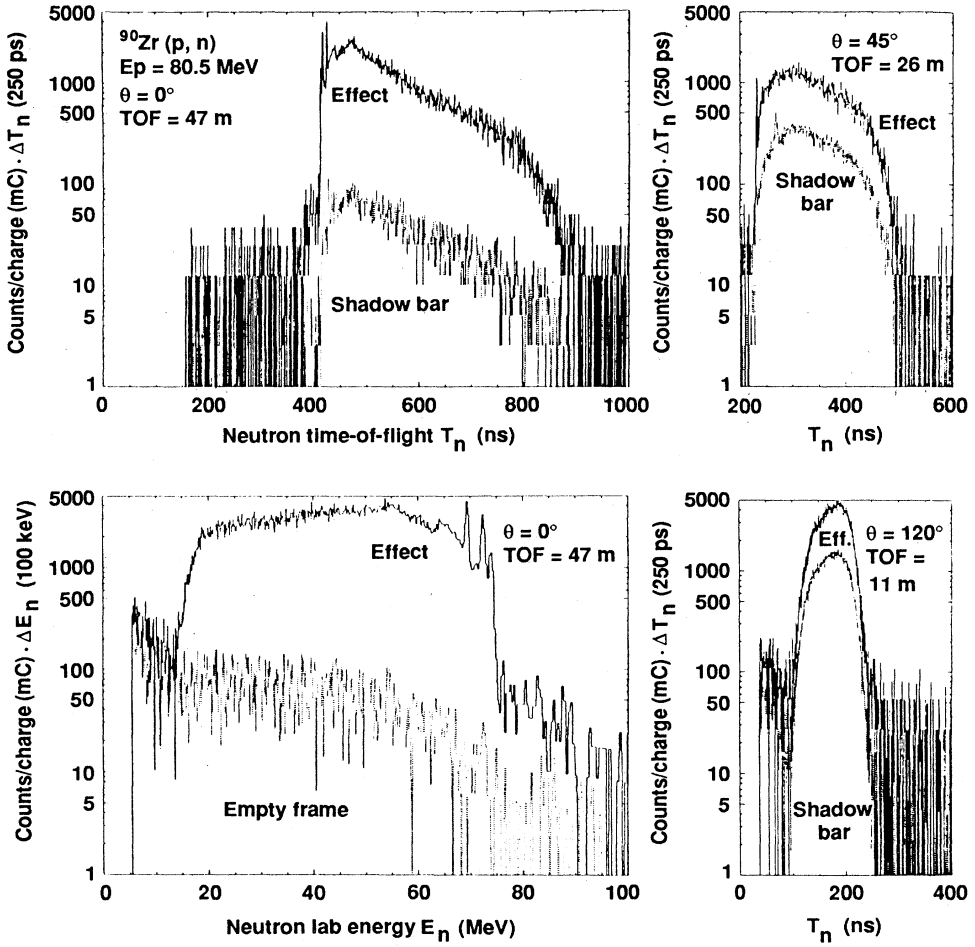

FIG. 2. tof spectra of "effect" and shadow bar run with detectors nos. 1, 3, and 5. The resulting energy spectra are shown for a run with and without target (bottom left).

with

$$\frac{d^2\sigma_{1i}}{dU_1 d\Omega_1} = \sum_L (2L+1) R_2(L) \rho_2(U) \left\langle \frac{d\sigma_L^{(\mathrm{DW})}}{d\Omega} \right\rangle . \quad (3)$$

The transition probabilities herein are calculated with DWBA matrix elements, viz.,

$$\frac{d^2 W_{n,n-1}}{dU\, d\Omega} = 2\pi^2 \rho_C(\mathbf{k}) \rho_2(U) |\langle \chi_n^- | V_{n,n-1} | \chi_{n-1}^+ \rangle|^2 . \quad (4)$$

For residual interaction $V_{n,n-1}$ in the DWBA matrix element, a finite-range Yukawa potential with $r_0 = 1$ fm has been chosen, whose strength V_0 was initially set to 25 MeV, in agreement with[14–16] the results $V_0 = 26 \pm 1$ MeV for low proton projectile energies. As Eq. (2) converged rapidly, the computations have been restricted to the first three steps of the SMDE chain.

The calculations revealed that the SMCE contributions are altogether negligibly small for $E_n > 20$ MeV. Therefore, only the SMDE contributions are presented in Fig. 5. The calculations for ^{90}Zr reproduce the angular distributions for three representative energies reasonably well over more than three orders of magnitude. However, the absolute values are off by a factor of 2. This discrepancy is far beyond the experimental uncertainties stated earlier. In particular, the detector efficiencies can be excluded as their origin, because (i) the discrepancy persists down to $E_n = 20$ MeV, where the efficiency calculations are based on very reliable input data, and (ii) the results of Kalend *et al.*[19] and this work agree well in the common forward angular range, if the cross sections are scaled[6] from $E_p = 90$ to 80 MeV.

We conclude therefore that V_0, the only relatively free parameter of the calculation, cannot be fixed to the value 25 MeV. A reduction of the effective nucleon-nucleon interaction strength to 20 MeV does indeed yield an overall agreement for the *whole* neutron range $E_n = 20$–70 MeV and both targets under consideration; see Fig. 5. Therefore, it seems improbable that this renormalization reflects an incorrect application of partial state densities $\rho_2(U)$ in Eq. (4) based on equidistant single-particle states. This agreement is not restricted to the angular distributions, but extends to all energy spectra (Fig. 6)

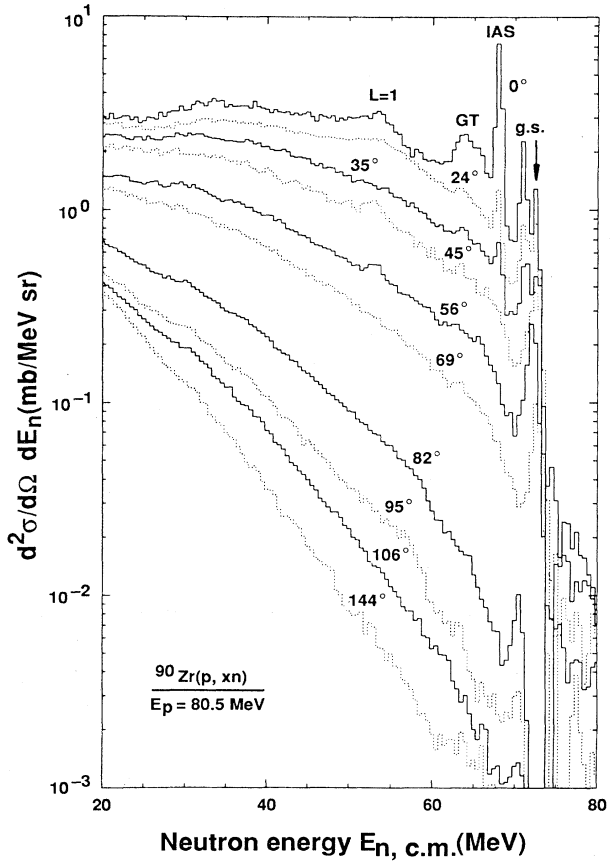

FIG 3. Selection of energy spectra for $^{90}Zr(p,xn)$.

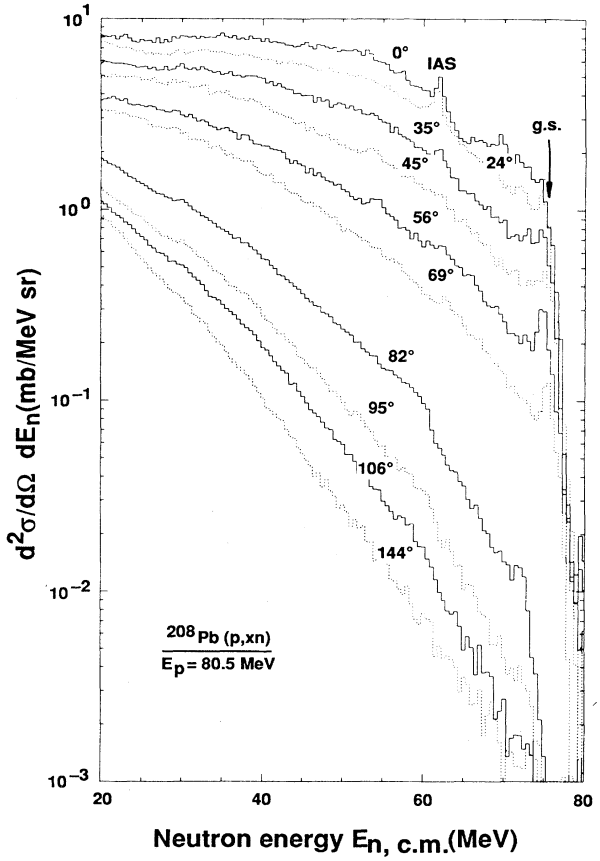

FIG. 4. Same as Fig. 3 for $^{208}Pb(p,xn)$.

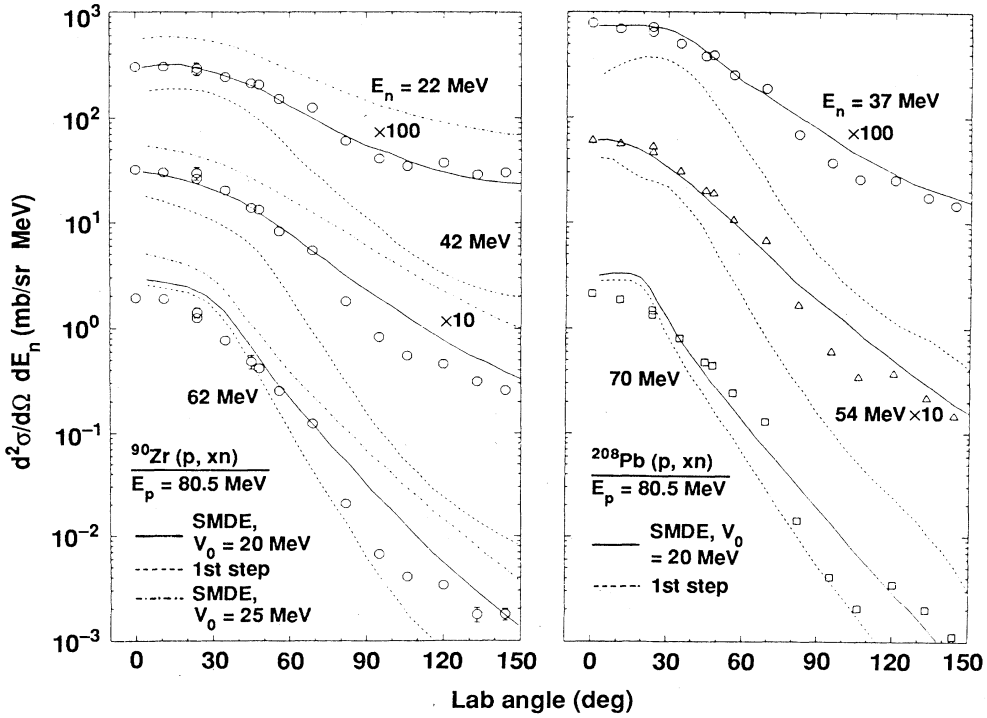

FIG. 5. Experimental angular distributions and SMDE calculations with effective nucleon-nucleon interaction V_0.

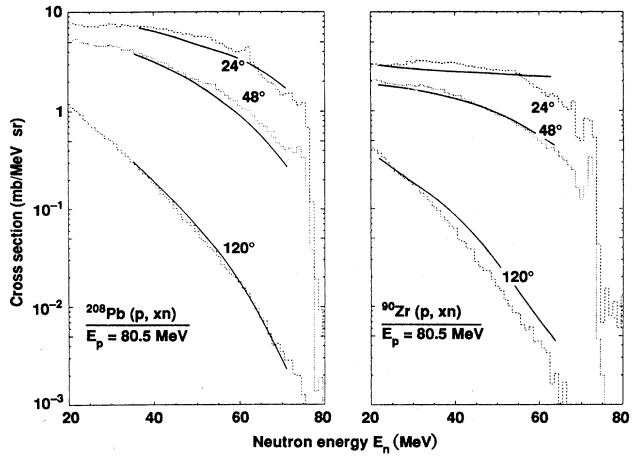

FIG. 6. Experimental neutron energy spectra compared to SMDE calculations with $V_0 = 20$ MeV.

with the exception of the high-energy range for ^{208}Pb(p,xn) at forward angles. In the latter region, the assumption of equidistant spacing and the $\rho_2(U)$ deduced are inadequate[22] in view of the strong shell effects in ^{208}Bi at low excitation U and the dominance of the single-step contribution. For higher angles, however, the higher steps are equally important, and this deficiency of $\rho_2(U)$ is masked by the integrations in Eq. (2).

If the first step of the SMDE really accounts for the main contribution at forward angles to the extent shown in Fig. 5, the scaling suggested for V_0 should be even more pronounced in direct transitions dominated by single-step nucleon-nucleon collisions. Evidence for such an energy dependence of the n-p effective interaction was indeed found by Kosugi *et al.*[23] in a DWBA analysis of the reactions ^{90}Zr $(p,d_{0,1,2})^{89}$Zr for $E_p = 20$–120 MeV. The spectroscopic factors they deduced decrease for an increase of E_p from 25 to 80 MeV by a factor ~ 2.25 corresponding to a factor of 1.5 for the interaction strength V_0.

For our continuous (p,n) spectra, we expect a reduction of V_0 smaller than a factor of 1.5 due to the contributions of higher steps and accordingly lower relative nucleon velocities. The value $\frac{25}{20} = 1.25$ found in this work fits into this qualitative trend. From the ongoing MSDE analysis of our data for $E_p = 120$ and 160 MeV (Ref. 38). We anticipate support for this interpretation.

B. Semiclassical and phenomenological models

In the geometry-dependent hybrid (GDH) model, the energy differential cross section for nucleon ejectiles ν of energy ϵ is[6]

$$\frac{d\sigma_\nu}{d\epsilon} = \pi \lambda\!\!\!^{-2} \sum_l (2l+1) T_l(\epsilon) \cdot P_{l\nu}(\epsilon) \ , \tag{5}$$

with a sum that extends over partial-wave contributions, each of which is proportional to the product of the transmission coefficient $T_l(\epsilon)$ and the emission probability $P_{l\nu}(\epsilon)$. The latter is calculated from Pauli-corrected partial-state densities, an emission rate into the continuum derived by means of the principle of detailed balance, and from intranuclear transition rates $\lambda_+^{NN}(\epsilon)$ leading via nucleon-nucleon collisions to states of increasing complexity. The Fermi energy, and transition rates $\lambda_+^{NN}(\epsilon)$ are the density-weighted average over the entrance channel trajectory for each partial wave l, whereas in the standard hybrid model the average is taken over the whole target nucleus such that Eq. (5) reduces to one term, namely $\sigma_R \cdot P_\nu(\epsilon)$.

These two models were applied to our data with the parameter values recommended as standard options in Ref. 6; in particular, a value $g = A/14$ MeV^{-1} corresponding to $a = A/8.5$ MeV^{-1} and pairing corrections according to Ref. 39 have been used. In Fig. 7, the results are compared with the experimental angle-integrated spectra. The overall agreement is within a factor of 2; the hybrid model reproduces the spectrum in the high-energy region, where single-step emission dominates, better than the GDH model, and for ^{90}Zr(p,xn) better than for ^{208}Pb. A similar tendency was observed in Ref. 19 at $E_p = 90$MeV. This may indicate an overestimation of the first step emission from the high partial waves in the GDH process. The excess of experimental yield in the Gamow-Teller (GT) and dipole ($L = 1$) resonance region over the procompound yield is not unexpected, because strength, in particular the spin-flip strength, is spread[40] and represents an additional contribution to the spectral continuum. The neglect of shell effects in the single-particle state density also enhances the discrepancy[22] for ^{208}Pb(p,xn).

Next, we turn to the angular distributions. The hybrid model has been extended to include the approach of classical intranuclear nucleon-nucleon scattering in a nucleon Fermi gas that is conceptually rigorous and avoids addi-

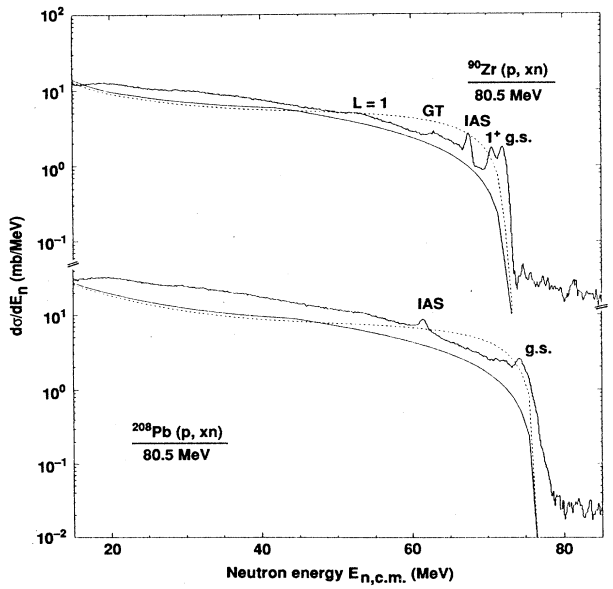

FIG. 7. Experimental angle-integrated energy spectra in comparison to calculations with standard (solid line) and geometry-dependent (dashed line) hybrid model.

tional assumptions wherever possible.[8] Application to the reaction ^{65}Cu(p,xn) for $E_p = 27$ MeV revealed[15] that this category of reaction models is not capable of reproducing the yield in the backward hemisphere. Figure 8 demonstrates that this discrepancy pertains to the projectile energy $E_p = 80$ MeV; we expect that it will continue to grow with projectile energy.[38]

Therefore, semiclassical PE models, in contrast to quantum-statistical ones,[11,12] have only little predictive power with respect to angular distributions. However, their reliable absolute cross section values $d\sigma/d\epsilon$ may be combined with systematics that parametrize the angular *shapes* as a function of projectile and/or ejectile type and energy. A first attempt of this type was presented in Ref. 41 in terms of a Legendre polynominal expansion, which worked reasonably well for nucleon energies up to about 45 MeV, but not beyond.[42] Neither was the application of that parametrization to our data successful. However, one of the previous authors reformulated that parametrization as[17]

$$\frac{d^2\sigma}{d\Omega\, d\epsilon} = a_0^{\mathrm{MSD}} \exp(a\cos\theta) + a_0^{\mathrm{MSC}}[\exp(a\cos\theta) + \exp(-a\cos\theta)] \,. \quad (6)$$

Here, a_0^{MSD} and a_0^{MSC} fix the absolute cross sections of the multistep direct and compound emission, respectively, and can be taken from a semiclassical PE model. The parametrization of the slope parameter $a(E_p,\epsilon)$ has been derived[17] from a large body of data for light ($A \leq 4$) projectiles with energies E_p up to 600 MeV. Here, Eq. (6) will be applied under the assumption of 100% MSD contribution with a_0^{MSD} being taken identical with the hybrid model value. Figure 8 demonstrates that the pronounced dependence of the angular shapes on the ejectile energy ϵ is fully reproduced and that the new parametrization is indeed superior to that of Ref. 41.

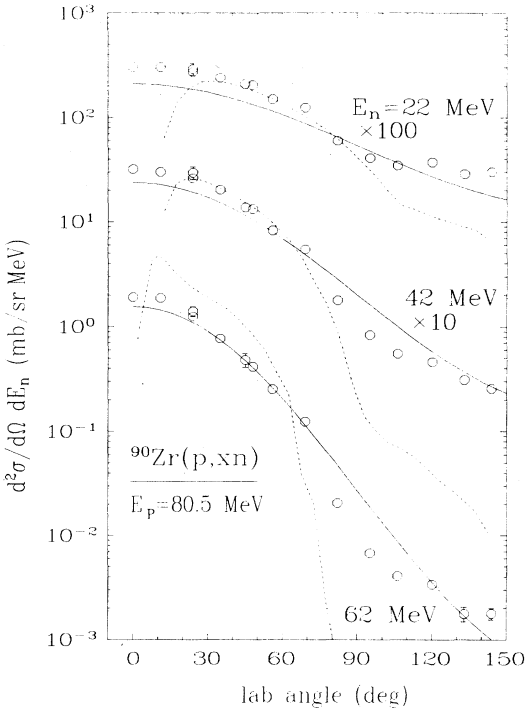

FIG. 8. Angular distributions for ^{90}Zr(p,xn) in comparison with the normalized results of Eq. (6) (solid line) and the hybrid model (dashed line).

IV. SUMMARY

The continuous neutron energy spectra of the reactions ^{90}Zr, ^{208}Pb(p,xn) have been measured for $E_p = 80.5$ MeV projectiles in the angular region $0° \leq \theta_{\mathrm{lab}} \leq 145°$ with emphasis on good resolution and low background.

The data show that the MSD mechanism is the dominant one for $E_n \geq 20$ MeV and that the higher step contributions are important even for the highest ejectile energies. The SMDE/SMCE model[12] is in very good agreement with these data if it is assumed that the effective nucleon-nucleon interaction V_0 is *not* constant but decreases with increasing projectile energy.

The standard hybrid model—as a prototype of a semiclassical model—with pairing corrections reproduces the angle-integrated spectra well within a factor of 2; however, the angular distributions cannot be described in terms of such a semiclassical nucleon-nucleon collision mechanism in a nuclear environment.

The predictive power of a recent phenomenological parametrization[17] for angular distribution in the spectral continuum over a broader range of energies is demonstrated with the present data.[38]

ACKNOWLEDGMENTS

The authors acknowledge the hospitality and cooperation of the Indiana University Cyclotron Facility (IUCF) staff for making this work possible. Discussions with Dr. C. Kalbach regarding systematics of angular distributions are appreciated.

*Present Address: Los Alamos Scientific Laboratory, Los Alamos, NM 87545.

[1]M. Blann, R. R. Doering, A. Galonsky, D. M. Patterson, and F. E. Serr, Nucl. Phys. **A257**, 15 (1976).

[2]S. M. Grimes, J. D. Anderson, and C. Wong, Phys. Rev. C **13**, 2224 (1976).

[3]W. A. Sterrenberg, S. M. Austin, E. E. P. Berg, R. DeVito, and A. Galonsky, Bull. Am. Phys. Soc. **24**, 649 (1979); A. Galonsky, in *The* (p,n) *Reaction and the Nucleon-Nucleon Force* (Plenum, New York, 1980), p. 191.

[4]W. Scobel, M. Blann, T. T. Komoto, M. Trabandt, S. M. Grimes, L. F. Hansen, C. Wong, and B. A. Pohl, Phys. Rev. C **30**, 1480 (1984).

[5]E. Gadioli and E. Gadioli-Erba, Nucl. Instrum. Methods **146**, 265 (1977).

[6]M. Blann and H. K. Vonach, Phys. Rev. C **28**, 1475 (1983).

[7]J. Bisplinghoff, Phys. Rev. C **33**, 1569 (1986); M. Blann and J. Bisplinghoff, Z. Phys. A **326**, 429 (1987).
[8]M. Blann, W. Scobel, and E. Plechaty, Phys. Rev. C **30**, 1493 (1984).
[9]H. Gruppelaar, P. Nagel, and P. E. Hodgson, Riv. Nuovo Cimento **9**, 1 (1986).
[10]K. Sato, Phys. Rev. C **32**, 647 (1985).
[11]T. Tamura, T. Udagawa, and H. Lenske, Phys. Rev. C **26**, 379 (1982).
[12]H. Feshbach, A. Kerman, and S. Koonin, Ann. Phys. (N.Y.) **125**, 429 (1980).
[13]R. Bonetti, L. Colli-Milazzo, and M. Melanotte, Phys. Rev. C **27**, 1003 (1983).
[14]R. Bonetti, M. DeCamnasio, L. Colli-Milazzo, and P. E. Hodgson, Phys. Rev. C **24**, 71 (1981).
[15]Y. Holler, A. Kaminsky, R. Langkau, W. Scobel, M. Trabandt, and R. Bonetti, Nucl. Phys. **A442**, 79 (1985).
[16]R. Bonetti and R. Colombo, Phys. Rev. C **28**, 980 (1983).
[17]C. Kalbach, Phys. Rev. C **37**, 2350 (1988).
[18]H. Sakai, K. Hatanaka, N. Matsuoka, T. Saito, A. Shimizu, T. Motobayashi, and T. Shibata, Phys. Lett. **133B**, **375** (1983).
[19]A. M. Kalend, B. D. Anderson, A. R. Baldwin, R. Madey, J. W. Watson, C. C. Chang, H. D. Holmgren, R. W. Koontz, J. R. Wu, and H. Machner, Phys. Rev. C **28**, 105 (1983).
[20]M. M. Meier, D. B. Holtkamp, G. L. Morgan, H. Robinson, G. J. Russell, E. R. Whitaker, W. Aiman and N. Paul, in the *Proceedings of the International Conference on Nuclear Data for Basic and Applied Science, Santa Fe, 1985,* edited by P. G. Young *et al.* (Gordon and Breach, New York, 1986), p. 1415; D. Filges (private communication).
[21]S. Cierjacks, Y. Hino, F. Raupp, L. Buth, D. Filges, P. Cloth, and T. W. Armstrong, Phys. Rev. C **36**, 1976 (1988); D. Filges, P. Cloth, T. W. Armstrong, S. Cierjacks, Y. Hino, F. Raupp, and L. Buth, *ibid.* **36**, 1988 (1987).
[22]K. Harder, A. Kaminsky, E. Mordhorst, W. Scobel, and M. Trabandt, Phys. Rev. C **36**, 834 (1987).
[23]S. Kosugi and T. Kosugi, Phys. Lett. **127B**, 389 (1983).
[24]D. L. Friesel, R. E. Pollock, T. Ellison, and W. P. Jones, Nucl. Instrum. Methods **B10/11**, 864 (1985).
[25]C. D. Goodman, C. C. Foster, H. B. Greenfield, C. A. Goulding, D. A. Lind, and J. Rapaport, IEEE Trans. Nucl. Sci. **26**, 2248 (1979).
[26]G. Randers-Pehrson, R. W. Finlay, and D. E. Carter, Nucl. Instrum. Methods **215**, 433 (1983).
[27]H. Schölermann and H. Klein, Nucl. Instrum. Methods **169**, 25 (1980).
[28]R. W. Finlay, C. E. Brient, D. E. Carter, A. Marcinkowski, C. Mellema, G. Randers-Pehrson, and J. Rapaport, Nucl. Instrum. Methods **198**, 197 (1982).
[29]R. A. Cecil, B. D. Anderson, and R. Madey, Nucl. Instrum. Methods **161**, 439 (1979).
[30]J. D'Auria, M. Dombsky, L. Moritz, T. Ruth, G. Sheffer, T. E. Ward, C. C. Foster, J. W. Watson, B. D. Anderson, and J. Rapaport, Phys. Rev. C **30**, 1999 (1984).
[31]T. N. Taddeucci, C. A. Goulding, T. A. Carey, R. C. Byrd, C. D. Goodman, C. Gaarde, J. Larsen, D. Horen, J. Rapaport, and E. Sugarbaker, Nucl. Phys. **A469**, 125 (1987).
[32]R. Byrd and W. C. Sailor (unpublished).
[33]Y. Holler, A. Kaminsky, B. Scharlemann, H. Krause, R. Langkau, W. Peters, G. Poppe, N. Schrim, W. Scobel, and R. Wien, Nucl. Instrum. Methods **A235**, 123 (1985).
[34]R. Madey, F. M. Waterman, A. R. Baldwin, J. Knudson, J. D. Carlson, and J. Rapaport, Nucl. Instrum. Methods **151**, 445 (1978).
[35]T. N. Taddeucci (private communiction).
[36]W. J. Courtney and J. D. Fox, At. Data Nucl. Data Tables **15**, 141 (1975).
[37]P. Schwandt, H. O. Meyer, W. W. Jacobs, A. D. Bacher, S. E. Vigdor, M. D. Kaitchuk, and R. T. Donoghue, Phys. Rev. C **26**, 55 (1982).
[38]M. Trabandt, M. Blann, R. Bonetti, R. C. Byrd, C. C. Foster, S. M. Grimes, B. A. Pohl, B. A. Remington, and W. Scobel, in *Proceedings of the Fifth International Conference of Nuclear Reaction Mechanisms, Varenna, 1988,* edited by E. Gadioli (Ricerca Scientifica ed Educazione Permanente, Milan, 1988), Supplemento 66, p. 52.